Nanospheres

Deutsche Ausgabe: DOI: 10.1002/ange.201601673
Internationale Ausgabe: DOI: 10.1002/anie.201601673

Synthesis of Highly Uniform Molybdenum–Glycerate Spheres and Their Conversion into Hierarchical MoS_2 Hollow Nanospheres for Lithium-Ion Batteries

Yawen Wang, Le Yu, and Xiong Wen (David) Lou**

Abstract: *Highly uniform Mo–glycerate solid spheres are synthesized for the first time through a solvothermal process. The size of these Mo–glycerate spheres can be easily controlled in the range of 400–1000 nm by varying the water content in the mixed solvent. As a precursor, these Mo–glycerate solid spheres can be converted into hierarchical MoS_2 hollow nanospheres through a subsequent sulfidation reaction. Owing to the unique ultrathin subunits and hollow interior, the as-prepared MoS_2 hollow nanospheres exhibit appealing performance as the anode material for lithium-ion batteries. Impressively, these hierarchical structures deliver a high capacity of about 1100 mAh g^{-1} at 0.5 A g^{-1} with good rate retention and long cycle life.*

Molybdenum disulfide (MoS_2) is a well-known two-dimensional (2D) material with graphene-like crystalline structure.[1–3] Recently, it has been recognized as a promising electrode material in the energy conversion and storage areas owing to its rich intercalation chemistry.[4–9] In particular, significant attention has been drawn on its potential use as the anode material in lithium-ion batteries (LIBs) because MoS_2 leads to a four-electron transfer reaction during the charge/discharge process with a high theoretical capacity of 669 mAh g^{-1}.[10–14] Nonetheless, it still faces some challenges in the practical applications such as the substantial volume change during cycling and poor rate performance. To solve these problems, various strategies have been reported to optimize the electrochemical performance of MoS_2 by rationally designing its geometric shapes and morphologies at nanoscale.[15–26]

Amongst the various approaches, the employment of hollow nanostructures has been considered as an attractive avenue to mitigate the above-mentioned obstacles and improve the lithium storage performance.[27,28] To be specific, the nanosized building blocks could effectively shorten the diffusion distance of Li^+ ions, relax the strain, and lower the barrier for lithium intercalation during the charge/discharge processes.[6,12,29] Meanwhile, the cavities in hollow structures ensure their high surface-to-volume ratio, which offers larger specific surface area for plenty of electrochemical active sites. Of note, the interior voids of the material could help preserve the integrity of the electrodes by accommodating the large volume variation associated with various electrochemical reactions.[30–33]

The templating method is the most common strategy to generate diverse hollow materials.[34–36] Usually, template-based synthesis involves the coating of the shell material on either hard or soft templates and the subsequent removal of the inner templates. For instance, we have recently prepared hollow MoS_2-carbon boxes using cubical Fe_2O_3 particles as a hard sacrificial template.[18] Despite its versatility, the templating method would face the potential incompatibility issue between the core and shell materials. A self-templating method, on the other hand, directly transforms a precursor template into the final product. Since it does not require the heterogeneous process, better control over the size uniformity can be easily achieved.[27,37] Self-templating approaches have been widely applied to generate a great variety of metal sulfides with distinct morphologies and compositions.[38–42] Recently, Zhang and co-workers developed an anion-exchange reaction of MoO_3-amine hybrid nanowires to produce hierarchical MoS_2 nanotubes.[5] However, such modified templating strategies have not been widely practiced yet owing to the paucity of applicable Mo-based templates with high size uniformity.

Herein we report the first synthesis of highly uniform Mo–glycerate (MoG) solid spheres by a facile solvothermal process. Afterwards, these MoG spheres are successfully sulfurized by thiourea in a mixed solvent to obtain the MoS_2 hollow nanospheres (HNS) constructed of nanosheets. The MoS_2 HNS are further annealed and applied as the anode materials for LIBs showing enhanced electrochemical performance.

The synthesis process is schematically illustrated in Figure 1. The whole synthesis process generally involves two stages. First, a solvothermal method is used to synthesize highly uniform MoG solid spheres using $MoO_2(acac)_2$ as the molybdenum source, and glycerol, isopropanol (IPA) together with a certain amount of water as the mixed solvent.[43] In the subsequent sulfidation step, sulfide (S^{2-}) ions released from thiourea at high temperature react with metal ions from the surface of the MoG spheres. Further anion exchange reaction between the inward diffusing S^{2-} ions and faster outward diffusing metal-ion species can create a void space between the newly formed MoS_2 layer and the inner MoG core.[31,39,43] Eventually after reaction for 6 h, the original MoG spheres have been chemically transformed into MoS_2 HNS composed of nanosheets.

[*] Dr. Y. Wang, Dr. L. Yu, Prof. X. W. Lou
School of Chemical and Biomedical Engineering
Nanyang Technological University
62 Nanyang Drive, Singapore 637459 (Singapore)
E-mail: xwlou@ntu.edu.sg
yule0001@e.ntu.edu.sg
Homepage: http://www.ntu.edu.sg/home/xwlou/

Supporting information for this article can be found under: http://dx.doi.org/10.1002/anie.201601673.

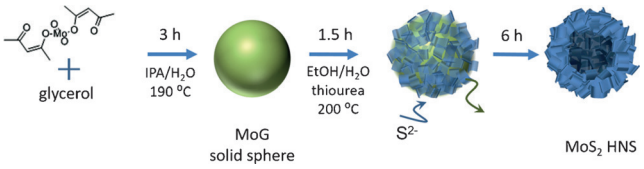

Figure 1. Schematic illustration of the formation process of the MoS_2 hollow sphere. Mo–glycerate (MoG) solid spheres were firstly formed by a solvothermal process, and then sulfurized by thiourea at 200 °C to obtain the MoS_2 hollow nanospheres (HNS).

Figure 2 shows the morphologies of the MoG precursor spheres and the as-formed MoS_2 HNS. Field-emission scanning electron microscope (FESEM) and transmission electron microscopy (TEM) images (Figure 2 a–c) show that the highly uniform MoG spheres are solid in nature with an average diameter of 580 nm. Besides, the well-separated spheres possess a rather smooth surface over the whole particle without any crystalline facets. Energy-dispersive X-ray (EDX) spectroscopy data confirms the existence of elements of Mo, C and O in the spheres (Figure S1, Supporting Information). The weak peaks of the X-ray diffraction (XRD) pattern imply the amorphous nature of the MoG spheres and the existence of possible MoO_2 phase (Figure S2, Supporting Information). Only a small loss in weight can be observed from the thermogravimetric analysis (TGA; Figure S3, Supporting Information), suggesting the small amount of organic components. The size and uniformity of the MoG spheres can be adjusted by tuning the volume fraction of water in the mixed solvent. Generally speaking, the spheres will grow bigger with compromised uniformity when the water content is reduced. While a slight increase of the water content to 37.5 vol% would still give uniform MoG spheres with a reduced average size of approximately 400 nm (Figure S4 a, Supporting Information). As the water content is reduced to 12.5 vol%, the MoG spheres obtained have an increased average size of about 1 μm (Figure S4 b, Supporting Information). In the absence of water, some irregular spheres with larger size could be obtained (Figure S4 c, Supporting Information). When the IPA/H_2O volume ratio is increased to 1, the MoG spheres experience a rapid reduction in size with much higher surface roughness (Figure S4 d, Supporting Information). Other Mo sources, such as $(NH_4)_6Mo_7O_{24}{\cdot}4H_2O$ and H_2MoO_4, could also be employed to generate MoG spheres. Nonetheless, the size distribution of corresponding products is quite difficult to control (Figure S5, Supporting Information).

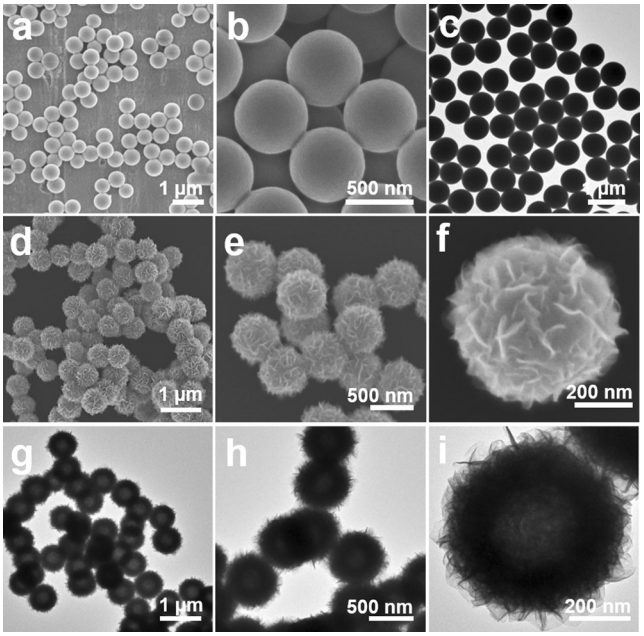

Figure 2. FESEM and TEM images of the a)–c) MoG solid spheres and d)–i) the corresponding hierarchical MoS_2 HNS after the sulfidation process.

After sulfidation under solvothermal conditions, the MoG spheres are converted into MoS_2 HNS. The panoramic FESEM image (Figure 2 d) indicates the overall spherical morphology of the as-prepared MoS_2 structures is well preserved with a uniform diameter of around 580 nm, almost same as the solid MoG spheres. The magnified observations (Figure 2 e,f) further reveal the surface of these hierarchical structures are constructed by nanosheet subunits. As depicted by TEM studies in Figure 2 g,h, the hollow structures and well-defined inner cavities of MoS_2 HNS are clearly elucidated by the sharp contrast between the center and the edge. From a closer examination of an individual sphere (Figure 2 i), it can be observed that the hierarchical shell has a thickness of about 140 nm. Moreover, the dark strips demonstrate the ultrathin nature of the exposed 2D nanosheets. XRD study of the hollow product (Figure S6, Supporting Information) can be assigned to the hexagonal phase of MoS_2, consistent with the previous reports.[5,44] In addition, the visible (002) diffraction peak further confirms the formation of a well-stacked layered structure of MoS_2. As determined by N_2 sorption measurement (Figure S7, Supporting Information), these MoS_2 HNS possess a Brunauer–Emmett–Teller specific surface area of 31.5 $m^2 g^{-1}$ with the pore sizes mostly below 10 nm.

To verify our hypothesis on the formation mechanism of the unique MoS_2 HNS, time series analysis is carried out to monitor the morphological evolution during the sulfidation reaction. The morphology of the MoG solid spheres appears unchanged and their surfaces remain smooth after heating treatment at 200 °C for 1 h (Figure S8 a, Supporting Information). When the solvothermal process prolongs to 1.5 h, a thin hierarchical shell made of MoS_2 nanosheets can be identified around the outermost layer of the spheres (Figure S8 b, Supporting Information). Over an extended period of 2 to 6 h, the continuous anion exchange reaction further supports the growth of the sulfurized shell accompanied by the formation of an obvious hollow interior within the spheres (Figure S8 c, Supporting Information). After the complete sulfidation process, the morphology of the hierarchical architectures will not change any more, even when the reaction is extended to 12 h (Figure S8 d, Supporting Information).

Figure 3 shows the FESEM and TEM images of the MoS_2 HNS after the thermal treatment at 700 °C in Ar/H_2 for 2 h. Despite the ultrathin feature, the FESEM images (Figure 3 a,b) indicate that the hierarchical MoS_2 shell exhibits

good structural stability to endure the harsh calcination conditions without apparent deformation in appearance. As elucidated by TEM observations in Figure 3c,d, the average size of the annealed HNS shrinks to about 450 nm with a reduced shell thickness about 100 nm. From the XRD pattern (Figure S9, Supporting Information), the crystallinity of the HNS increases significantly after annealing. All Bragg peaks can be indexed to the MoS_2 phase (JCPDS card no. 37–1492).[18] No residues or impurity phases are detected, further demonstrating complete transformation of the MoG spheres after sulfidation. In agreement with the XRD analysis, the inter-layer spacing of 0.66 nm and a distinct set of visible lattice fringes with an inter-planar distance of 0.27 nm can be clearly observed in the high resolution TEM (HRTEM) images, which are consistent with the expanded *d* spacing

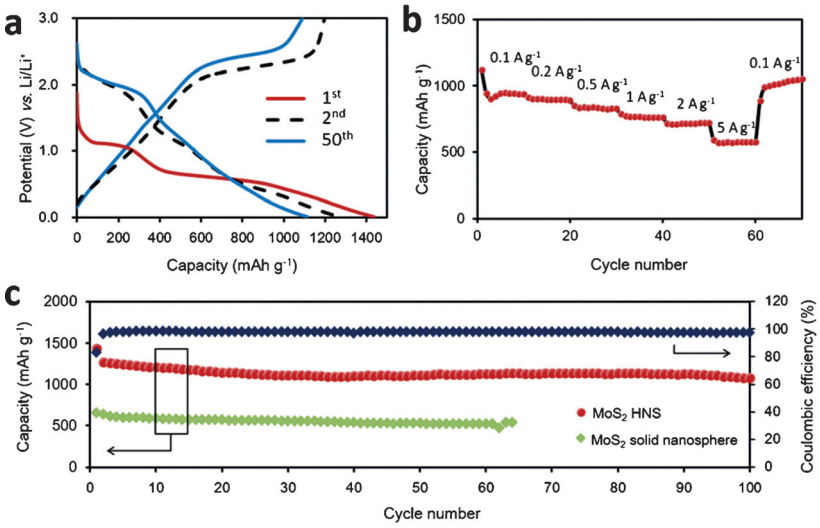

Figure 4. a) Charge–discharge voltage profiles at 0.5 $A g^{-1}$, b) rate capability test, and c) cycling performance at 0.5 $A g^{-1}$ of the MoS_2 HNS and of MoS_2. The blues trace shows Coulombic efficiency of MoS_2 HNS.

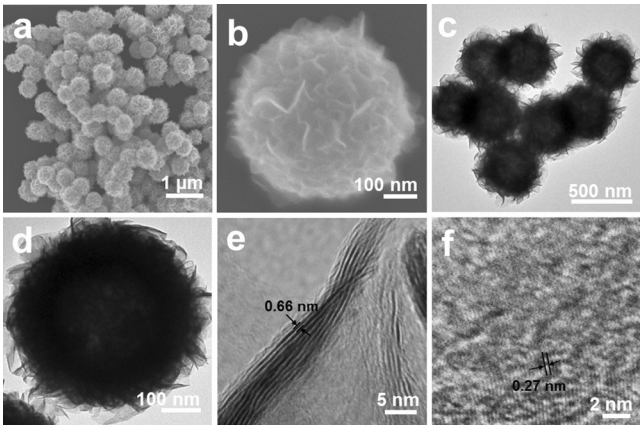

Figure 3. a),b) FESEM and c),d) TEM images of the MoS_2 HNS after annealing in Ar/H_2 at 700 °C for 2 h. e),f) HRTEM images of the MoS_2 sheets.

of the (002) planes and (100) facet of hexagonal MoS_2 (Figure 3e,f).

The hollow MoS_2 HNS were evaluated as the anode material for LIBs to demonstrate their promising application. Figure 4a shows the representative galvanostatic charge/discharge voltage profiles of the hollow nanospheres in the voltage range of 0.01–3.0 V versus Li/Li^+ at a current density of 0.5 $A g^{-1}$. Two voltage plateaus located at 1.1 and 0.6 V can be observed in the first discharge, corresponding, respectively to the formation of Li_xMoS_2 by the insertion of Li^+ ions into the interlayer MoS_2 lattice and the generation of Li_2S and Mo through the further reaction between Li_xMoS_2 and Li^+.[15,45,46] In the first charge process, a pronounced peak at around 2.3 V can be assigned to the delithiation of Li_2S to sulfur. In the following discharge process, the discharge plot with two voltage plateaus located at 2.0 and 1.3 V is observed, indicating a multi-step lithium insertion mechanism.[16,47,48] To further study the mechanism of lithium storage, the cyclic voltammograms (CV) curves of the hollow nanospheres (Figure S10, Supporting Information) obtained at various cycles are investigated. In the CV plots, the representative cathodic/anodic peaks can be clearly identified, which is consistent with the above charge-discharge voltage profiles. In addition, the CV profiles are approximately overlapping except for the initial cycle, suggesting the excellent stability of these hollow structures for reversible lithium storage. Galvanostatic charging-discharging measurements confirm that these unique MoS_2 HNS can be reversibly cycled at various current densities. As shown in Figure 4b, the average specific capacities of the hollow nanospheres are approximately 944, 895, 831, 762, 711 and 576 mAh g^{-1} at the current densities of 0.1, 0.2, 0.5, 1, 2 and 5 $A g^{-1}$, respectively. When the current density is reduced back to 0.1 $A g^{-1}$, a high capacity of 1000 mAh g^{-1} is immediately resumed, suggesting the good reversibility of the electrode materials. The cycling performance of the MoS_2 HNS electrodes is presented in Figure 4c. The reversible capacity of the MoS_2 hollow nanospheres in the first cycle is 1270 mAh g^{-1}, which is much higher than that of solid MoS_2 spheres (640 mAh g^{-1}). The irreversible capacity of 238 mAh g^{-1} in the first cycle corresponding to a Coulombic efficiency (CE) of 83% could be attributed to irreversible processes such as the formation of the solid-electrolyte interface (SEI) film and decomposition of electrolyte.[14,20] The MoS_2 HNS deliver a reversible specific capacity of 1100 mAh g^{-1} at 0.5 $A g^{-1}$ without obvious capacity decay after 100 cycles, while the reversible specific capacity of solid MoS_2 sample is only 500 mAh g^{-1}. The Coulombic efficiencies of MoS_2 HNS are nearly 100% after the first few cycles. The superior electrochemical performance of the hollow spheres might be related to the increment of electrochemical active sites compared with the solid sample. Clearly, the hierarchical MoS_2 HNS exhibit interesting properties as potential anode materials for LIBs benefitting from their unique structural features such as the ultrathin subunits and well-defined hollow interior to withstand the structural strain.

In summary, we have developed a facile solvothermal method to synthesize highly uniform Mo–glycerate spheres with size in the range of 400–1000 nm. These Mo–glycerate spheres can be used as precursor to synthesize MoS_2 hollow nanospheres constructed of nanosheets. The process allows good quality control on the uniformity and structure of the obtained MoS_2 materials. After thermal treatment in inert environment, hollow MoS_2 nanospheres show excellent electrochemical performance as the anode of lithium-ion batteries with high specific capacities and excellent cycling stability. It is worth mentioning that the ease of the structural tailoring provides the possibilities to further optimize the properties of the MoS_2-based functional materials.

Acknowledgements

X.W.L. acknowledges funding support from the Ministry of Education of Singapore through Academic Research Fund (AcRF) Tier-1 Funding (M4011154.120; RG12/13).

Keywords: hollow structures · lithium-ion batteries · MoS_2 · nanosheets · nanospheres

How to cite: *Angew. Chem. Int. Ed.* **2016**, *55*, 7423–7426
Angew. Chem. **2016**, *128*, 7549–7552

[1] X. Huang, Z. Zeng, H. Zhang, *Chem. Soc. Rev.* **2013**, *42*, 1934.
[2] M. Xu, T. Liang, M. Shi, H. Chen, *Chem. Rev.* **2013**, *113*, 3766.
[3] Q. H. Wang, K. Kalantar-Zadeh, A. Kis, J. N. Coleman, M. S. Strano, *Nat. Nanotechnol.* **2012**, *7*, 699.
[4] J. F. Xie, H. Zhang, S. Li, R. X. Wang, X. Sun, M. Zhou, J. F. Zhou, X. W. Lou, Y. Xie, *Adv. Mater.* **2013**, *25*, 5807.
[5] S. F. Zhuo, Y. Xu, W. W. Zhao, J. Zhang, B. Zhang, *Angew. Chem. Int. Ed.* **2013**, *52*, 8602; *Angew. Chem.* **2013**, *125*, 8764.
[6] T. Stephenson, Z. Li, B. Olsen, D. Mitlin, *Energy Environ. Sci.* **2014**, *7*, 209.
[7] X. Xu, W. Liu, Y. Kim, J. Cho, *Nano Today* **2014**, *9*, 604.
[8] M. Chhowalla, H. S. Shin, G. Eda, L.-J. Li, K. P. Loh, H. Zhang, *Nat. Chem.* **2013**, *5*, 263.
[9] Z. M. Wan, J. Shao, J. J. Yun, H. Y. Zheng, T. Gao, M. Shen, Q. T. Qu, H. H. Zheng, *Small* **2014**, *10*, 4975.
[10] K. Chang, W. Chen, *ACS Nano* **2011**, *5*, 4720.
[11] J. Xiao, X. J. Wang, X. Q. Yang, S. D. Xun, G. Liu, P. K. Koech, J. Liu, J. P. Lemmon, *Adv. Funct. Mater.* **2011**, *21*, 2840.
[12] C. Zhu, X. Mu, P. A. van Aken, Y. Yu, J. Maier, *Angew. Chem. Int. Ed.* **2014**, *53*, 2152; *Angew. Chem.* **2014**, *126*, 2184.
[13] S. K. Das, R. Mallavajula, N. Jayaprakash, L. A. Archer, *J. Mater. Chem.* **2012**, *22*, 12988.
[14] H. Hwang, H. Kim, J. Cho, *Nano Lett.* **2011**, *11*, 4826.
[15] L. Yang, S. Wang, J. Mao, J. Deng, Q. Gao, Y. Tang, O. G. Schmidt, *Adv. Mater.* **2013**, *25*, 1180.
[16] X. Zhou, L.-J. Wan, Y.-G. Guo, *Chem. Commun.* **2013**, *49*, 1838.
[17] L. Zhang, X. W. Lou, *Chem. Eur. J.* **2014**, *20*, 5219.
[18] X. Y. Yu, H. Hu, Y. Wang, H. Chen, X. W. Lou, *Angew. Chem. Int. Ed.* **2015**, *54*, 7395; *Angew. Chem.* **2015**, *127*, 7503.
[19] L. Zhang, H. B. Wu, Y. Yan, X. Wang, X. W. Lou, *Energy Environ. Sci.* **2014**, *7*, 3302.
[20] J. Zhou, J. Qin, X. Zhang, C. Shi, E. Liu, J. Li, N. Zhao, C. He, *ACS Nano* **2015**, *9*, 3837.
[21] D. B. Kong, H. Y. He, Q. Song, B. Wang, W. Lv, Q. H. Yang, L. J. Zhi, *Energy Environ. Sci.* **2014**, *7*, 3320.
[22] J. Shao, Q. T. Qu, Z. M. Wan, T. Gao, Z. C. Zuo, H. H. Zheng, *ACS Appl. Mater. Interfaces* **2015**, *7*, 22927.
[23] Q. T. Qu, F. Qian, S. M. Yang, T. Gao, W. J. Liu, J. Shao, H. H. Zheng, *ACS Appl. Mater. Interfaces* **2016**, *8*, 1398.
[24] J. Wang, J. L. Liu, D. L. Chao, J. X. Yan, J. Y. Lin, Z. X. Shen, *Adv. Mater.* **2014**, *26*, 7162.
[25] H. Jiang, D. Y. Ren, H. F. Wang, Y. J. Hu, S. J. Guo, H. Y. Yuan, P. J. Hu, L. Zhang, C. Z. Li, *Adv. Mater.* **2015**, *27*, 3687.
[26] S. P. Zhang, B. V. R. Chowdari, Z. Y. Wen, J. Jin, J. H. Yang, *ACS Nano* **2015**, *9*, 12464.
[27] X. Y. Yu, L. Yu, X. W. Lou, *Adv. Energy Mater.* **2015**, *6*, 1501333.
[28] X. Y. Lai, J. E. Halpert, D. Wang, *Energy Environ. Sci.* **2012**, *5*, 5604.
[29] C. Liu, F. Li, L. P. Ma, H. M. Cheng, *Adv. Mater.* **2010**, *22*, E28.
[30] N. Liu, Z. D. Lu, J. Zhao, M. T. McDowell, H. W. Lee, W. T. Zhao, Y. Cui, *Nat. Nanotechnol.* **2014**, *9*, 187.
[31] P. P. Wang, H. Y. Sun, Y. J. Ji, W. H. Li, X. Wang, *Adv. Mater.* **2014**, *26*, 964.
[32] S. M. Xu, C. M. Hessel, H. Ren, R. B. Yu, Q. Jin, M. Yang, H. J. Zhao, D. Wang, *Energy Environ. Sci.* **2014**, *7*, 632.
[33] S. Li, J. J. Niu, Y. C. Zhao, K. P. So, C. Wang, C. A. Wang, J. Li, *Nat. Commun.* **2015**, *6*, 7872.
[34] Y. S. Li, J. L. Shi, *Adv. Mater.* **2014**, *26*, 3176.
[35] J. B. Joo, Q. Zhang, I. Lee, M. Dahl, F. Zaera, Y. D. Yin, *Adv. Funct. Mater.* **2012**, *22*, 166.
[36] J. W. Nai, Y. Tian, X. Guan, L. Guo, *J. Am. Chem. Soc.* **2013**, *135*, 16082.
[37] Q. Zhang, W. Wang, J. Goebl, Y. Yin, *Nano Today* **2009**, *4*, 494.
[38] D. R. Cummins, H. B. Russell, J. B. Jasinski, M. Menon, M. K. Sunkara, *Nano Lett.* **2013**, *13*, 2423.
[39] S. L. Xiong, H. C. Zeng, *Angew. Chem. Int. Ed.* **2012**, *51*, 949; *Angew. Chem.* **2012**, *124*, 973.
[40] L. Yu, B. Y. Xia, X. Wang, X. W. Lou, *Adv. Mater.* **2016**, *28*, 92.
[41] X. Y. Yu, L. Yu, H. B. Wu, X. W. Lou, *Angew. Chem. Int. Ed.* **2015**, *54*, 5331; *Angew. Chem.* **2015**, *127*, 5421.
[42] W. W. Zhao, C. Zhang, F. Y. Geng, S. F. Zhuo, B. Zhang, *ACS Nano* **2014**, *8*, 10909.
[43] L. Shen, L. Yu, H. B. Wu, X.-Y. Yu, X. Zhang, X. W. Lou, *Nat. Commun.* **2015**, *6*, 6694.
[44] L. N. Ye, C. Z. Wu, W. Guo, Y. Xie, *Chem. Commun.* **2006**, 4738.
[45] J.-Z. Wang, L. Lu, M. Lotya, J. N. Coleman, S.-L. Chou, H.-K. Liu, A. I. Minett, J. Chen, *Adv. Energy Mater.* **2013**, *3*, 798.
[46] C. Wang, W. Wan, Y. Huang, J. Chen, H. H. Zhou, X. X. Zhang, *Nanoscale* **2014**, *6*, 5351.
[47] C. Zhang, Z. Wang, Z. Guo, X. W. Lou, *ACS Appl. Mater. Interfaces* **2012**, *4*, 3765.
[48] L. Wang, Z. Xu, W. Wang, X. Bai, *J. Am. Chem. Soc.* **2014**, *136*, 6693.

Received: February 17, 2016
Published online: April 20, 2016

